

Atomic resolution imaging of beryl: an investigation of the nano-channel occupation

V. ARIVAZHAGAN*, F. D. SCHMITZ†,‡, P. E. VULLUM§, ||, A. T. J. VAN HELVOORT§ & B. HOLST*

*Department of Physics and Technology, University of Bergen, Bergen, Norway

†German Gemmological Association, Idar-Oberstein, Germany

‡Centre for Gemstone Research, FB 09 Institute for Geosciences, Johannes Gutenberg-University of Mainz, Mainz, Germany

§Department of Physics, Norwegian University of Science and Technology, Trondheim, Norway

||SINTEF Materials and Chemistry, Trondheim, Norway

Key words. Beryl, colour centre, HAADF STEM, nano-channel, transmission electron microscopy.

Summary

Beryl in different varieties (emerald, aquamarine, heliodor etc.) displays a wide range of colours that have fascinated humans throughout history. Beryl is a hexagonal cyclo-silicate (ring-silicate) with channels going through the crystal along the *c*-axis. The channels are about 0.5 nm in diameter and can be occupied by water and alkali ions. Pure beryl ($\text{Be}_3\text{Al}_2\text{Si}_6\text{O}_{18}$) is colourless (variety goshenite). The characteristic colours are believed to be mainly generated through substitutions with metal atoms in the lattice. Which atoms that are substituted is still debated it has been proposed that metal ions may also be enclosed in the channels and that this can also contribute to the crystal colouring. So far spectroscopy studies have not been able to fully answer this. Here we present the first experiments using atomic resolution scanning transmission electron microscope imaging (STEM) to investigate the channel occupation in beryl. We present images of a natural beryl crystal (variety heliodor) from the Bin Thuan Province in Vietnam. The channel occupation can be visualized. Based on the image contrast in combination with *ex situ* element analysis we suggest that some or all of the atoms that are visible in the channels are Fe ions.

Introduction

The atomic structure of beryl ($\text{Be}_3\text{Al}_2\text{Si}_6\text{O}_{18}$) was first resolved by X-ray diffraction in 1926 (Bragg & West, 1926) and later refined (Gibbs *et al.*, 1968). Beryl is a hexagonal cyclo-silicate (ring silicate) (see Fig. 1). It consists of regular six-membered silicate rings of SiO_4 tetrahedra that link latterly

and vertically to adjacent rings by tetrahedral beryllium (Be) and octahedral aluminium (Al). Six-membered silicate rings form open channels along the crystallographic *c*-axis with a diameter of around 0.5 nm. This is so big that alkali ions as well as water molecules can be trapped in the channels (Folinsbee, 1941; Vorma *et al.*, 1965; Hawthorne & Cerny, 1977; Sherriff *et al.*, 1991; Andersson, 2006). The dynamic of water molecules trapped in the nano-channels has been investigated using neutron scattering and various spectroscopy methods (Gorshunov *et al.*, 2013; Anovitz *et al.*, 2013; Zhukova *et al.*, 2014; Kolesnikov *et al.*, 2016). Isotope analysis of the trapped water has been used to obtain information about the geological conditions at the time of crystal formation (Beal & Lentz, 2010) and to investigate historical emerald trade routes (Giuliani *et al.*, 2000). It has been proposed that single nitrogen atoms could be enched within the lattice channels as a candidate for qubits for quantum computer applications (Mashkovtsev & Thomas, 2005).

Beryl in its pure form is colourless (variety goshenite) (Mathew *et al.*, 2000), but exists in a large variety of colours. Numerous spectroscopy studies have been performed to investigate this including infrared spectroscopy (Mathew *et al.*, 1997), Mössbauer spectroscopy, Raman spectroscopy (Charoy *et al.*, 1996), UV/Vis/NIR spectroscopy, electron paramagnetic resonance and electron spin echo spectroscopy (Mashkovtsev *et al.*, 2010, see also Fridrichová *et al.*, 2015 and references therein). It is known that the colour stems from the incorporation of various metal atoms (Fritsch & Rossman, 1988), for example, chrome (the classical emerald; Wood & Nassau, 1968), iron (aquamarine; Goldman *et al.*, 1978 and heliodor – sometimes referred to as golden beryl; Wood & Nassau, 1968; Loeffler & Burns, 1976; Goldman *et al.*, 1978), vanadium (green beryl – also sometimes referred to as emerald; Wood & Nassau, 1968) and manganese (bixbite and red beryl – sometimes referred to as morganite; Wood & Nassau, 1968;

Authors V. Arivazhagan and F. D. Schmitz contributed equally.

Correspondence to: Bodil Holst, Department of Physics and Technology, University of Bergen, Allegaten 55, 5007 Bergen, Norway. Tel: +47 55 58 29 67; e-mail: bodil.holst@uib.no

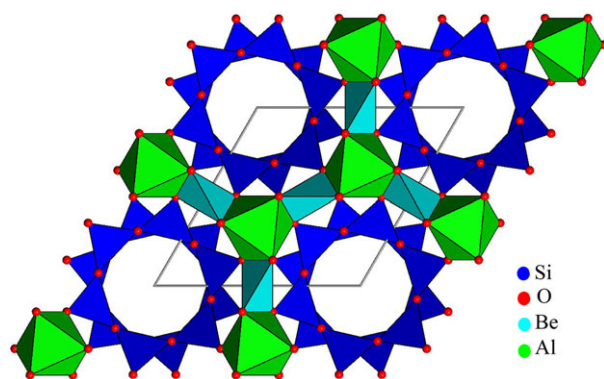


Fig. 1. Atomic model of beryl.

Shigley & Foord, 1984). How this incorporation takes place and how it affects the colouring, is still a matter of debate. In the case of incorporation of iron, the resulting colour change varies from the characteristic blue in aquamarine over bluish to yellowish green to deep golden in heliodor.

The yellow colour of heliodor is due to absorption between 450 nm and the absorption edge at 320 nm. The cause for this was originally attributed to the substitution of Fe³⁺ ions for Al³⁺ ions in the octahedral Al positions in the crystal (Wood & Nassau, 1968). Later it was proposed that both Fe²⁺ and Fe³⁺ are incorporated in the octahedral positions of Al (Spinolo *et al.*, 2007). Other studies claimed that the yellow colour of heliodor is in fact linked to a substitution of Fe³⁺ on a tetrahedral site, that is, Be or Si (Solntsev & Bukin, 1997; Andersson, 2013). For further recent work on natural beryl crystals see Huong *et al.* (2012) and Fridrichová *et al.* (2015).

It has been suggested that metal atoms/ions can also be trapped in the channels. This has been proposed as an explanation for certain colour variations in beryl (Viana *et al.*, 2002). However, other studies suggest that metal atoms in the channels do not contribute to the colouring at all. For example Mathew *et al.* report measurements on samples of colourless beryl (goshenite), which showed a strong Fe³⁺ signal in Mössbauer spectroscopy (Mathew *et al.*, 2000). If the Fe³⁺ ions had been substituted into the lattice structure one would have expected a visible colour change.

Despite the geological and gemmological interest no electron microscopy work at genuine atomic resolution has been carried out on beryl so far. This is presumably due to its fragility and the fact that it is beam sensitive, which makes both sample preparation and imaging difficult. TEM images of a natural beryl from Mexico can be found in (Buseck & Iijima, 1974). The lattice images are of high quality but give only the overall structure. Given the TEM instrumentation and the technique chosen it is not apparent if channels are empty or filled.

In this paper, we present the first aberration corrected atomic resolution high-angle annular dark-field (HAADF) scanning transmission electron microscopy (STEM) images of a natural beryl crystal. This technique has a supreme



Fig. 2. Image of the beryl crystal sample used for this work, a natural heliodor from the Bin Thuan Province in Vietnam. The crystal is 2.49 cm long and has a weight of 7.65 Karat. The red patches are remains of the host rock.

spatial resolution and the contrast makes it possible to differentiate between variations in the average atomic number of the columns as well as filling of the channels. In 'Experimental methods' section, we present the experimental methods applied, including the TEM specimen preparation as this is a crucial step in obtaining the results. In 'Results and analysis' section, the results are presented, including an element analysis on the bulk crystal sample based on energy dispersive X-ray spectroscopy (EDX) and induction coupled plasma mass spectrometry (ICP-MS). The study gives the overall structure and the local variations in the channels.

Experimental methods

The sample investigated here is a natural beryl crystal of the heliodor variety from the Bin Thuan Province in Vietnam. The crystal is 2.49 cm long and has a weight of 7.65 Karat (see Fig. 2). In a preliminary study, an element analysis of 59 natural beryl samples from 13 different countries was performed (Schmitz). This sample was chosen because the element analysis shows that it has a low amount of nonformula elements compared to the other samples, except for Fe and Na.

TEM specimen preparation and imaging

A TEM foil taken from a (0001) facet was prepared on a Helios Nanolab Dual-Beam Focused Ion Beam (FIB) (FEI, Hillsboro, Oregon, USA). Because of the poor electrical conductivity of beryl, the macroscopic single crystal was coated by a 40 nm thick Pt/Pd layer prior to FIB preparation to avoid charging in the FIB. In the FIB, an additional 200 nm Pt protection layer was deposited by electron beam-assisted deposition, before adding a 2 μm thick carbon protection layer by ion beam-assisted deposition. All coarse ion beam thinning was done at 30 kV acceleration voltage for the Ga⁺ ions. Final thinning was performed at 5 and 2 kV acceleration voltages to minimize the ion-induced surface damage on either side of the TEM foil.

The TEM lamella had no additional coating and was even in thickness. All conducting layers were on the side of beryl material, and the electron beam propagated through beryl only, that is, no additional conductive layer added for TEM analysis. The area imaged was 40 ± 20 nm thick.

TEM was performed with a double Cs corrected, cold FEG JEOL ARM200CF, operated at 200 kV. The high angle, annular dark field (HAADF) STEM images were acquired with collection angle range of 43–170 mrad. The beam convergence semicollection angle was 27.4 mrad.

Element analysis

The element analysis was carried out on the bulk crystal sample using two different instruments. The concentrations of the main elements (Si, Al, Fe and Na) were measured with an electron-microprobe (EMPA) of the type JEOL JXA-8200 using energy dispersive X-ray spectroscopy (EDX). The EMPA was equipped with a Xe-gas and a pentaerythritol (PET)-detector. The other main elements: Be and O and H from water in the channels cannot be measured with this instrument because these three elements are all too light. Further a trace element analysis was performed with an inductively coupled plasma quadrupole mass spectrometer (ICP-MS) of the type NWR 193 (ESI New Wave) 193 nm Agilent 7500, calibrated with the standard NIST-SRM 610. Si was measured with the EMPA to form the internal standard for the trace element analysis. For each instrument, 10 measurements were carried out on 10 different positions chosen at random. Different positions were chosen for the two instruments.

Results and analysis

Figure 3 shows a raw atomic resolution HAADF STEM image of beryl taken along the *c*-axis. The 60 pA was the highest beam current that could be used to avoid sample damage during high resolution scanning transmission electron microscopy (STEM) imaging. Even at 60 pA, the combination of a small pixel size (< 0.1 Å) and a high pixel dwell time (> 30 μs) still resulted in significant beam damage. The total tolerable dose limits the achievable resolution (i.e. ‘Rose’s Criterion’) (Van Dyck *et al.*, 2004; Egerton, 2013). Nevertheless due to the higher inherent contrast of HAADF STEM compared to conventional bright-field TEM imaging, a high spatial resolution could still be achieved. A reduction of the electron beam acceleration voltage from 200 to 80 kV significantly increased the electron beam-induced sample damage, rather than reducing it. This indicates, as expected for low atomic number minerals, that the electron beam-induced damage mechanism is radiolysis rather than knock-on damage (Williams & Carter, 2009). It was not possible to collect sufficient signal for element analysis on individual atoms using X-ray energy dispersive spectroscopy (EDX) and/or electron energy loss spectroscopy (EELS) due to this low critical dose for this beryl sample. How-

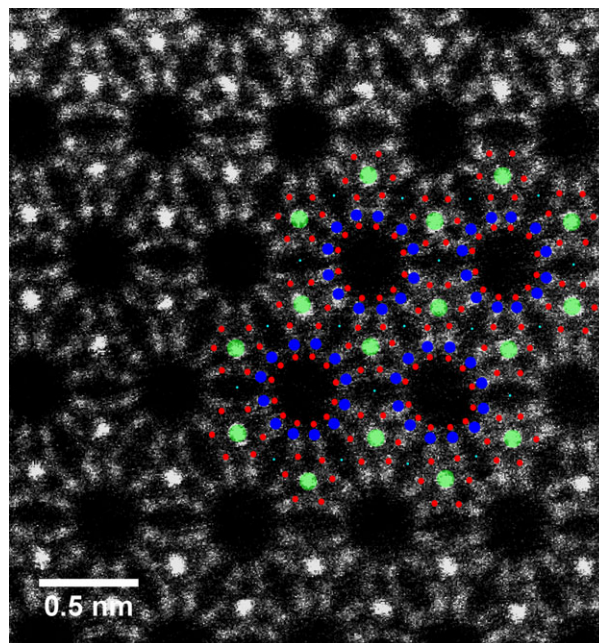


Fig. 3. Atomic resolution HAADF STEM image of a natural Heliodor crystal along the *c*-axis. Be atoms are not visible. The colour code for the atomic model superimposed on the image is similar to that used in the atomic model presented in Figure 1.

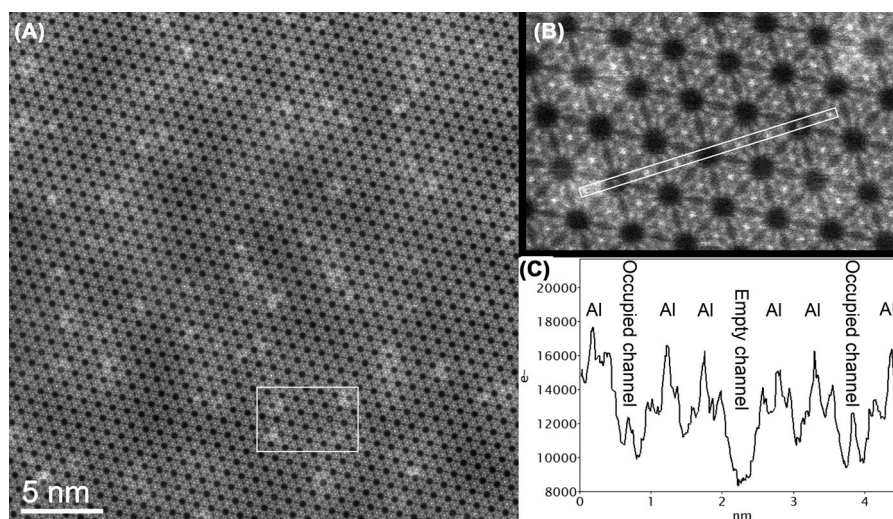
ever, a significant amount of information can still be extracted from the image contrast. It is well known that the HAADF signal intensity scales almost with the atomic number Z squared ($I \approx Z^{1.6-2.0}$), often referred to as Z -contrast imaging (Nellist & Pennycook, 2000). This, given an even specimen thickness for the FIB lamella, together with the incoherent imaging, often allows a direct interpretation of the lattice. These are key advantages over high resolution transmission electron microscopy (HRTEM). Hence, for beryl with the ideal chemical formula $\text{Be}_3\text{Al}_2(\text{Si}_2\text{O}_6)_3$, the atomic columns containing Al ($Z = 13$) and Si ($Z = 14$) are expected to dominate the image contrast. At first glance, it might appear strange that the Al columns are so much brighter than the Si columns. This is however due to the fact that there are 12 Si columns per unit cell along the present $[0001]$ projection of the structure, but only two Al-columns. For every Si atom in one of the Si columns, there are two Al atoms in each of the Al columns. The Be columns appear dark due to the low atomic number ($Z = 4$), but the O columns ($Z = 8$) are visible. This is due to the average low atomic number in the sample and the high number density of atoms in the O columns. The overall structure is in excellent agreement with the atomic model for beryl.

Table 1 shows the results of the trace element analysis, including the results for the concentrations of the main elements obtained with EMPA (EDX). In order to calculate the concentrations of the trace elements, the concentrations of all the main elements must be known as well. Following the standard procedure in the literature, we assume that the

Table 1. Element analysis of the heliodor crystal sample used for this work. All elements above the detection limit are listed. Following the common approach we include the wt.% numbers of the oxides for the EDX analysis. Fe has been taken to be trivalent. See main text for details.

EMPA (EDX)					
Element-oxide	Concentration oxide [wt.%]	Error [wt.%]	Element	Element concentration [wt.%]	Error [wt.%]
SiO ₂	66.3	0.2	Si	30.99	0.09
Al ₂ O ₃	18.1	0.1	Al	9.58	0.06
Fe ₂ O ₃	0.23	0.03	Fe	0.16	0.02
Na ₂ O	0.085	0.01	Na	0.063	0.007
–	–	–	Cs	0.04	0.015
<i>BeO and H₂O estimated</i>	<i>13 (BeO) 2 (H₂O)</i>		<i>Be H</i>	<i>4.68 0.11</i>	
<i>Sum</i>	<i>99.7</i>	<i>0.35</i>			

ICP-MS		
Element	Element-concentration [ppm]	Error [ppm]
Li	340	20
Na	600	60
Mg	5	1
Sc	18.5	4
Ti	45	3
Zn	26	2
Ga	15	1
Rb	4.1	0.2
Cs	325	20
<i>Sum without Na</i>	<i>780</i>	<i>40</i>

**Fig. 4.** (A) Atomic resolution dark field TEM image of a natural Heliodor crystal along the *c*-axis. Individual atoms can be seen in the centre of some of the nano-channels. (B) Enlarged image of box marked in (A). (C) Intensity line profile of box marked in (B).

BeO concentration is 13 wt.% (the value corresponding to the ideal beryl formula) and the H₂O concentration is 2 wt.% (Deer *et al.*, 1986; Viana *et al.*, 2002). Following the standard convention, we also include calculated oxide values based on the experimentally determined wt.% with Fe taken to be trivalent and values for Na₂O also included. Strictly speaking, this is

not quite correct since the Na atoms are not included directly in the lattice, but are present as ions in the channels and further we may have both Fe²⁺ and Fe³⁺ in the lattice as well as some Fe atoms present as ions in the channels. The ICP-MS analysis combined with the EMPA analysis tells us that the concentration of most nonformula elements is very low

and can be ignored. The only significant contributions are: Fe ($Z = 26$): 160 ppm, Na ($Z = 11$): 600 ppm, Cs ($Z = 55$): 325 ppm and Li ($Z = 3$): 340 ppm. Na, Cs and Li are all alkali metals and thus expected to be included as ions in the channels. Note that the number of Cs atoms is small compared to the other alkali atoms. For every Cs atom there is 10.6 ± 0.2 Na atoms.

Figure 4 shows a larger scale, raw atomic resolution HAADF image, along the c -axis together with an enlarged section and a line scan intensity plot. Here it can be seen that several channels contain what appear to be individual atoms centred in the middle of the channels. As discussed in the introduction it is known from spectroscopy that the channels in beryl can contain alkali ions. According to the element analysis presented above the only alkali metals present here in larger amounts are Na, Cs and Li. Further as also discussed in the introduction it has been speculated that Fe ions ($Z = 26$) can be incorporated in the channels. Li is too light to be imaged even in this sample by HAADF STEM. Cs is heavier, but only present in a very small amount. Na is lighter than both Al and Si, and a few Na atoms in some of the open channels would not have the scattering power to give the observed contrast in the channels unless these channels are close to fully occupied by Na ions. However, such a high occupancy of Na ions is excluded based on the overall Na content in the sample (roughly one Na atom for every 32 channels in each atomic plane). Fe is the only trace elements that has both the scattering power ($Z = 26$) and is present with a sufficient concentration (roughly one Fe atom for every 35 channels in each atomic plane) to be able to cause the observed HAADF intensity in some of the channels. However, it cannot be excluded that Na and/or Cs contribute to some of the contrast in the partly filled channels. Fe incorporated in the lattice has not been analysed in this study, due to the relatively poor signal to noise ratio between atomic columns of the same type, enforced by the low critical dose.

Conclusion and future work

In this paper, the first atomic resolution HAADF STEM images of a natural beryl crystal are presented. It is possible to image ions centred in the nano-channels. All formula atoms, except Be are clearly visible. The low critical dose hampers TEM analysis and makes spectroscopy analysis impossible. However, the Z -contrast suggests that Fe atoms are present in the channels. Our results give interesting perspectives for future work. An obvious next step would be a systematic, combined HAADF STEM/spectroscopy study of other varieties of beryl and quantitative analysis combined with image simulations to determine if metal ions trapped in the channels contribute to the colour generation. It should be possible to do this through Z -contrast imaging alone. Imaging in the direction perpendicular to the c -axis (e.g. $[1 \ -2 \ 1 \ 0]$) should also be included for complementary information. More efficient spectrometers

would maybe allow elemental analysis on individual atoms to be performed below the critical electron dose, and thereby it should be possible to determine conclusively the cause of specific colour changes.

Acknowledgements

This project was supported by the Research Council of Norway through the program ForNy2020, project nr. 234159/O30 and support to the Norwegian Micro- and Nano-Fabrication, NorFab (197411/V30) and the NORTEM (197405) facilities as well as the Norwegian PhD Network on Nanotechnology for Microsystems (VA research grant).

References

- Andersson, L.O. (2013) The yellow color center and trapped electrons in beryl. *Can. Miner.* **51**, 15–25.
- Andersson, L.O. (2006) The positions of H, Li and Na impurities in beryl. *Phys. Chem. Miner.* **33**, 403–416.
- Anovitz, L.M., Mamontov, E., Ishai, P.B. & Kolesnikov, A.I. (2013) Anisotropic dynamics of water ultraconfined in macroscopically oriented channels of single-crystal beryl: a multifrequency analysis. *Phys. Rev. E* **88**, 1–16
- Beal, K.-L. & Lentz, D.R. (2010) Aquamarine beryl from Zealand Station, Canada: a mineralogical and stable isotope study. *J. Geosci.* **55**, 57–67.
- Bragg, W.L. & West, J. (1926) The structure of beryl, $\text{Be}_3\text{Al}_2\text{Si}_6\text{O}_{18}$. *P. Roy. Soc. Lond. A. Mat.* **111**, 691–714.
- Buseck, P.R. & Iijima, S. (1974) High resolution electron microscopy of silicates. *Am. Miner.* **59**, 1–21.
- Charoy, B., De Donato, P., Barres, O. & Pinto-Coelho, C. (1996) Channel occupancy in an alkali-poor beryl from Serra Branca (Goias, Brazil): spectroscopic characterization. *Am. Miner.* **81**, 395–403.
- Deer, W.A., Howie, R.A. & Zussman, J. (1986) *Rock Forming Minerals: Disilicates and Ring Silicates*. Longman Scientific & Technical, London, England.
- Egerton, R.F. (2013) Control of radiation damage in the TEM. *Front. Elect. Microsc. Mater. Sci.* **127**, 100–108.
- Folinsbee, R.E. (1941) Optic properties of cordierite in relation to alkalis in the cordierite-beryl structure. *Am. Miner.* **26**, 485–500.
- Fridrichová, J., Bacík, P., Rusinová, P., Antal, P., Skoda, R., Bizovská, V. & Miglierini, M. (2015) Optical and crystal-chemical changes in aquamarines and yellow beryls from Thanh Hoa province, Vietnam induced by heat treatment. *Phys. Chem. Miner.* **42**, 287–302.
- Fritsch, E. & Rossman, G. (1988) An update on color in gems, part III: colors caused by band gaps and physical phenomena. *Gems Gemol.* **24**, 81–102.
- Gibbs, G.V., Breck, D.W. & Meagher, E.P. (1968) Structural refinement of hydrous and anhydrous synthetic beryl, $\text{Al}_2(\text{Be}_3\text{Si}_6)\text{O}_{18}$ and emerald, $\text{Al}_{1.9}\text{Cr}_{0.1}(\text{Be}_3\text{Si}_6)\text{O}_{18}$. *Lithos* **1**, 275–285.
- Giuliani, G., Chaussidon, M., Schubnle, H.-J. *et al.* (2000) Oxygen isotopes and emerald trade routes since antiquity. *Science* **287**, 631–633.
- Goldman, D.S., Rossman, G.R. & Parkin, K.M. (1978) Channel constituents in beryl. *Phys. Chem. Miner.* **3**, 225–235.

- Gorshunov, B.P., Zhukova, E.S., Torgashev, V.I. *et al.* (2013) Quantum behavior of water molecules confined to nanocavities in gemstones. *J. Phys. Chem. Lett.* **4**, 2015–2020.
- Hawthorne, F.C. & Cerny, P. (1977) The alkali-metal positions in Cs-Li beryl. *Can. Miner.* **15**, 414–421.
- Huong, L.T., Häger, T., Hofmeister, W. *et al.* (2012) Gemstones from Vietnam: an update. *Gems Gemol.* **48**, 158–176.
- Kolesnikov, A.I., Reiter, G.F., Choudhury, N. *et al.* (2016) Quantum tunneling of water in beryl: a new state of the water molecule. *PRL* **116**, 1–6.
- Loeffler, B.M. & Burns, R.G. (1976) Shedding light on the color of gems and minerals. *Am. Sci.* **64**, 636–647.
- Mashkovtsev, R.I., Kulik, L.V. & Solntsev, V.P. (2010) Silver atoms in the structural channels of beryl. *J. Struct. Chem.* **51**, 869–874.
- Mashkovtsev, R.I. & Thomas, V.G. (2005) Nitrogen atoms encased in cavities within the beryl structure as candidates for qubits. *Appl. Magn. Reson.* **28**, 401–409.
- Mathew, G., Karanth, R.V., Gundo Rao, T. K. & Desphande, R.S. (2000) Colouration in natural beryls: a spectroscopic investigation. *J. Geol. Soc. Ind.* **56**, 285–303.
- Mathew, G., Karanth, R.V., Gundo Rao, T.K. & Desphande, R.S. (1997) Channel constituents of alkali-poor Orissan beryls: an FT-IR spectroscopic study. *Curr. Sci.* **73**, 1004–1011.
- Nellist, P.D. & Pennycook, S.J. (2000) The principles and interpretation of annular dark-field Z-contrast imaging. *Adv. Imag. Elect. Phys.* **113**, 147–203.
- Schmitz, F. PhD Thesis, in preparation. Institute for Geosciences; Johannes Gutenberg-University of Mainz.
- Sherriff, L.S., Grundy, H.D., Hartmann, J.S., Hawthorne, F.C. & Cerny, P. (1991) The incorporation of alkalis in beryl: multi-nuclear MAS NMR crystal-structure studies. *Can. Miner.* **29**, 271–285.
- Shigley, J.E. & Foord, E.E. (1984) Gem-quality red beryl from the Wah-Wah Mountains, Utah. *Gems Gemol.* **20**, 208–221.
- Solntsev, V.P. & Bukin, G.V. (1997) The color of natural beryls from rare-metal Mozambique pegmatites. *Russ. Geol. Geophys.* **38**, 1661–1668.
- Spinolo, G., Fontana, I. & Galli, A. (2007) Optical absorption spectra of Fe²⁺ and Fe³⁺ in beryl crystals. *Phys. Stat. Sol.* **244**, 4660–4668.
- Van Dyck, D., Van Aerts, S. & Den Dekker, A.J. (2004) Physical limits on atomic resolution. *Microsc. Microanal.* **10**, 153–157.
- Viana, R.R., Da Costa, G.M., De Grave, E., Jordt-Evangelista, H. & Starn, W.B. (2002) Characterization of beryl (aquamarine variety) by Mössbauer spectroscopy. *Phys. Chem. Miner.* **29**, 78–86.
- Vorma, A., Shama, T.G. & Haapala, I. (1965) The alkali-metal positions in Cs-Li beryl. *CR Soc. Geol. Finlande.* **37**, 119–129.
- Williams, D.B. & Carter, C.B. (2009) *Transmission Electron Microscopy*. Springer Verlag, Springer, New York, USA.
- Wood, D.L. & Nassau, K. (1968) The characterization of beryl and emerald by visible and infrared absorption spectroscopy. *Am. Miner.* **53**, 777–800.
- Zhukova, E.S., Torgashev, V.I., Gorshunov, B.P. *et al.* (2014) Vibrational states of a water molecule in a nano-cavity of beryl crystal lattice. *J. Chem. Phys.* **140**, 1–11